Photochemical Charge Separation within Aromatic Hydrazines and the Effect of Excited-State Intervalence in Dihydrazines

Stephen F. Nelsen,*,‡ Asgeir E. Konradsson,‡ Michael N. Weaver,‡ Ilia A. Guzei,‡ Mark Goebel,§ Rüdiger Wortmann,*,†,§ Jenny V. Lockard,|| and Jeffrey I. Zink||

Contribution from Department of Chemistry, University of Wisconsin, 1101 University Avenue, Madison, Wisconsin 53706-1396, Department of Chemistry, Physical Chemistry, Kaiserslautern University of Technology, Erwin-Schrödinger-Strasse, D-67663 Kaiserslautern, Germany, and Department of Chemistry and Biochemistry, University of California, Los Angeles, Box 9515569, Los Angeles, California 90095-1569

Received: May 23, 2005; In Final Form: September 30, 2005

Photolysis into the longest wavelength absorption band of 2-*tert*-butyl-2,3-diazabicyclo[2.2.2]oct-3-yl hydrazine (Hy) substituted naphthalenes causes aryl group reduction electron transfer to give $^{+}$Hy−Ar^{-}. Electrooptical absorption measurements characterize the charge separation properties from these bands. Emission studies demonstrate that the separation between absorption and emission maxima for symmetrically disubstituted compounds is smaller than that for monosubstituted compounds, which is attributed to excited-state intervalence. The excited-state diabatic surfaces may be described as a Hy^{+}−NA^{-} −Hy^{0}, Hy^{0}−NA^{-}−Hy^{+} pair, for which electronic interaction produces a double minimum that qualitatively resembles that in the ground state of the disubstituted intervalence radical cations.

Introduction

We have used the 2-*tert*-butyl-2,3-diazabicyclo[2.2.2]oct-3-yl hydrazine group (Hy) previously as a charge-bearing unit to prepare symmetrically disubstituted localized intervalence radical cations having aromatic bridges, abbreviated $^{+}$Hy−Ar−Hy. For several Ar groups, including durenediyl (2,3,5,6-tetramethyl-1,4-benzenediyl, DU), 4,4′-biphenyldiyl (BI), and naphthalene-1,4-diyl (NA), the electron transfer (ET) rate constant at a

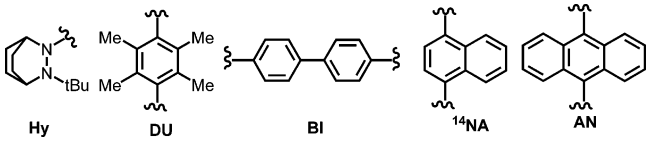

convenient temperature is near the value of 10^{8} $M^{-1}s^{-1}$ that is required to measure it accurately by ESR using the nitrogen splitting constant.[1] This allowed comparison to the value predicted from the optical spectrum using the simple classical two-state Marcus−Hush theory.[2] In the simplest treatment, identical energy structures that have charge localized on each of the two charge-bearing units in the hypothetical absence of electronic coupling are represented as diabatic energy surfaces *a* and *b* that are parabolas with minima at zero and one on the electron-transfer coordinate, *x*, having the vertical separation at these minima of the vertical reorganization energy, λ. The electronic interaction between the charge-bearing units through the bridge, represented by the electronic matrix coupling element for superexchange, H_{ab}, is used as the off-diagonal element in a simple two-state Hamiltonian. The ground and excited adiabatic surfaces (here designated 1 and 2) obtained by solving for energy represent the energy surfaces that are actually present, with the electronic coupling intact. This model makes the ET barrier $\Delta G^{*} = \lambda/4 - H_{ab} + H_{ab}^{2}/\lambda$.[2] Both parameters may be estimated from the optical spectrum because the transition energy of the charge-transfer band at the band maximum, E_a, is equal to λ, and H_{ab} is evaluated from the transition dipole moment for this band, μ_{12}, and the change in dipole moment upon electron transfer on the diabatic surfaces, $\Delta\mu_{ab}$, using Hush's formula, $H_{ab} = (\mu_{12}/\Delta\mu_{ab})E_a$.[2a] In this treatment $\Delta\mu_{ab} = ed_{ab}$, requiring estimation of the electron-transfer distance on the diabatic surfaces, d_{ab}, which is not obtainable from the absorption spectrum. There has been some confusion in the literature between d_{ab} and the distance on the ground-state adiabatic surface, here called d_{12}. In our later previous work we use the generalized Mulliken−Hush theory of Cave and Newton,[3] which allows conversion of a d_{12} estimate into the d_{ab} value required for Marcus−Hush theory using the optical absorption spectrum because $d_{ab} = [\Delta\mu_{12}^{2} + 4\mu_{12}^{2}]^{1/2}/e$. The experimental shape of the observed charge-transfer band for intervalence bis-hydrazines was fit using a quartic term to augment the usual parabolic diabatic surfaces,[4] and d_{ab} was estimated using the triplet state dipolar splitting of the related diradical dication as a model for d_{12},[1] or the d_{12} estimate was obtained using semiempirical calculations.[5] Surprisingly good agreement of the predicted and observed rate constants was found. This demonstrates that the Marcus−Hush treatment can be rather accurate, even when H_{ab} is large enough to make the ET essentially adiabatic.[1] The anthracene-bridged compound 9,10-Hy$_2$AN^{+}, however, had an ET rate constant over 100 times that expected using the classical two-state Marcus−Hush theory, and its optical spectrum showed that this occurs because the excited-state having symmeterical charge distribution corresponding to bridge oxidation (ET to give Hy−AN^{+}−Hy) lies too close in energy to the hydrazine-centered $^{+}$Hy−AN−Hy ground state for the two-state model to be accurate.[6]

In the present work, we consider photoelectron transfer induced by irradiation into the longest wavelength absorption

* Corresponding author. E-mail: nelsen@chem.wisc.edu.
† Deceased March 13, 2005.
‡ Department of Chemistry, University of Wisconsin.
§ Department of Chemistry, Physical Chemistry, Kaiserslautern University of Technology.
|| Department of Chemistry and Biochemistry, University of California, Los Angeles.

10.1021/jp052702m CCC: $30.25
Published on Web 11/10/2005

TABLE 1: X-ray and B3LYP/6-31+G*-Calculated Geometries of Monohydrazines

compound	Hy^1NA		Hy^2NA		Hy^9AN
method	X-ray[a]	DFT	X-ray	DFT	DFT
d(NN), Å	1.446(6)	1.460	1.458(2)	1.453	1.457
d(NC_{Ar}), Å	1.442(6)	1.435	1.495(2)	1.430	1.434
N−Ar twist, deg	50.2(6)	49.0	37.1(2)	36.0	51.8
$\Delta\alpha_{av}(N_{Ar})$, deg	9.3(4)	7.4	7.8(1)	7.0	4.9
$\Delta\alpha_{av}(N_{t-Bu})$, deg	6.8(4)	6.1	6.3(1)	6.0	6.4

[a] Average of two crystallographically independent enantiomeric structures in the unit cell are given.

band of the neutral oxidation level of the three Hy-substituted monohydrazines shown below, as well as the four symmetrically substituted dihydrazine naphthalenes shown. Both electrooptical

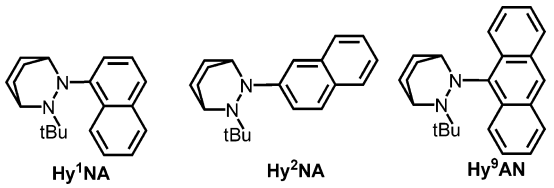

absorption, which allows one to determine $\Delta\mu_{12}$, and emission

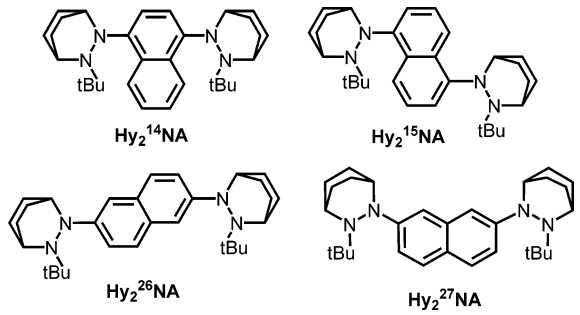

spectroscopy studies have been done to probe photoinduced charge separation in these molecules.

Results

Structural Studies. An important difference between α- and β-substituted compounds is that nonbonded steric interactions force a larger twist between the nitrogen lone pair and the aromatic ring for the former. This decrease in conjugation also results in slightly greater pyramidality for the nitrogens of Hy^1NA. Parameters from the X-ray structures of the monohydrazine-substituted naphthalenes and some hybrid HF-density functional theory calculations using B3LYP/6-31+G* (labeled DFT)[7] are summarized in Table 1. The N-aryl twist entry is the average of the NN,aryl and the bridgehead N,aryl′ dihedral angles (for Hy^1NA, the NN,C_1C_2 and C_αN,C_1C_9 angles), and the $\Delta\alpha_{av}$ entry is 120° minus the average of the heavy atom bond angles at nitrogen. $\Delta\alpha_{av}$ is 0° for a planar nitrogen and 10.5° for a tetrahedral one, and $\Delta\alpha_{av}$ is close to linear with formal fractional s character of the lone pair, causing the lone pair ionization energy to be calculated to be nearly linear with $\Delta\alpha_{av}$. Table 1 shows data for the most stable conformations, that with the NN bond syn to C_2 for Hy^1NA and syn to C_1 for Hy^2NA, which are the conformations present in the crystals. The diastereomeric conformation for Hy^2NA that has NN syn to C_3 is calculated to lie 0.30 kcal/mol higher in enthalpy using B3LYP/6-31G* and 0.27 kcal/mol higher by the presumably less accurate semiempirical AM1 method.[8] As for the Hy_2Ar compounds studied previously,[1] the relative orientation of the two Hy units with respect to each other is not important, so diastereomeric conformations with the *tert*-butyl groups syn and anti to each other are close in enthalpy.

TABLE 2: Lowest-Energy Absorption Band Characteristics (in Dioxane)

compound	λ_{max} nm	E_a cm^{-1}	ϵ_{max} $M^{-1}cm^{-1}$	μ_{12} D[a]
Hy^1NA	346	28 900	3510	2.19
Hy^2NA	353	28 330	2209	1.49
Hy^9AN	459	21 790	3730	2.29
$Hy_2{}^{14}NA$	386	25 930	5030	2.37
$Hy_2{}^{15}NA$	362	27 620	7338	2.85
$Hy_2{}^{26}NA$	378	26 460	2845	1.60
$Hy_2{}^{27}NA$	360	27 780	1459	0.99

[a] These values include the factor of 0.89 refractive index correction for dioxane.[10]

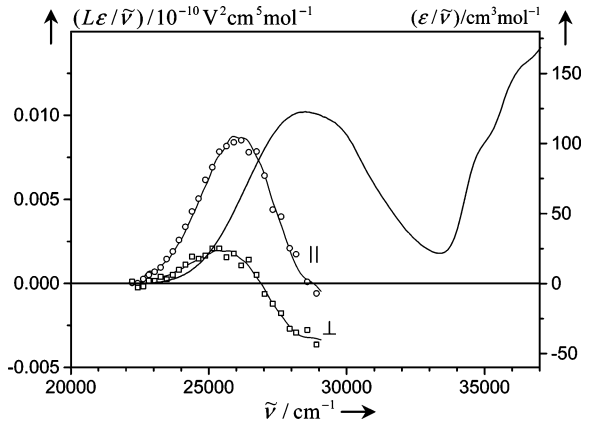

Figure 1. Electrooptical ($L\epsilon/\tilde{\nu}$) and optical ($\epsilon/\tilde{\nu}$) absorption spectra of Hy^1NA in dioxane solution at $T = 298$ K. Experimental data points are shown for parallel (○) and perpendicular (□) polarization of the incident light relative to the applied static field along with fit curves obtained by multilinear regression analysis.

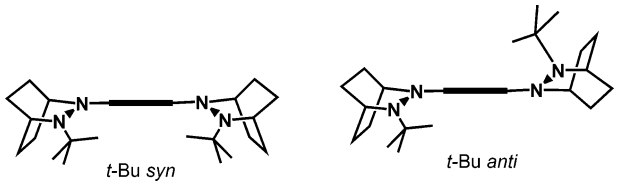

Electrooptical Absorption Measurements (EOAM). The optical absorption spectra of the monhydrazines exhibit broad and structureless first absorption bands near 350 nm for the naphthalene derivatives and at 459 nm for Hy^9AN. Integration of the absorption spectrum, $\epsilon/\tilde{\nu}$, yielded rather small transition dipole moments, μ_{12}. The results for all seven compounds are listed in Table 2. We used the equation discussed by Liptay to obtain μ_{12},[9] but with the addition of the refractive index (n) correction of $3n^{1/2}/(n^2 + 2) = 0.89$ for dioxane, which was pointed out to be desirable for considering charge transfer by the Kodak group.[10] To investigate the charge-transfer character of these low-lying bands, we carried out EOAM experiments in dioxane solution at $T = 298$ K. The EOAM spectral plots of $L\epsilon/\tilde{\nu}$ for Hy^1NA and Hy^9AN are displayed along with the optical absorption spectra, $\epsilon/\tilde{\nu}$, in Figures 1 and 2.

In an electrooptical absorption experiment, one observes the influence of the static external electric field on the absorbance of a dilute solution of a chromophore in an inert solvent. The observed change of the absorbance is related to the change of the molar decadic absorption coefficient, ϵ, of the solute induced by the field. The effect of a uniform external electric field, E_e,

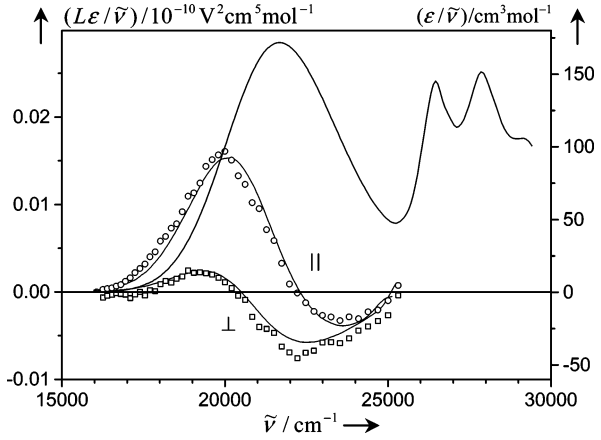

Figure 2. Electrooptical ($L\epsilon/\tilde{\nu}$) and optical ($\epsilon/\tilde{\nu}$) absorption spectra of Hy[9]AN in dioxane solution at $T = 298$ K. The legend is the same as that in Figure 1.

on the absorption coefficient, ϵ, can be described by the quantity L[9]

$$L = L(\varphi, \tilde{\nu}) = (1/E_e^2)[\epsilon^E(\varphi, \tilde{\nu}) - \epsilon(\tilde{\nu})]/\epsilon(\tilde{\nu}) \quad (1)$$

Here ϵ and ϵ^E denote the molar absorption coefficient in the absence and presence of the applied field, respectively, φ is the angle between the direction of E_e and the electric field vector of the incident light, and $\tilde{\nu}$ is the wavenumber. Usually the quantity L is measured at two polarizations, $\varphi = 0°$ and 90°, and for several wavenumbers in the absorption band. The EOAM spectrum is then represented in the form $L\epsilon/\tilde{\nu}$ and analyzed by multilinear regression in terms of the optical absorption spectrum, $\epsilon/\tilde{\nu}$, and its first and second derivative. The regression yields a set of coefficients[11] that may be approximated here as

$$E = (f_0/kT)^2\mu_1^2(3\cos^2\phi - 1) \quad (2)$$

$$F = (f_0^2/kT)\mu_1\Delta\mu_{12}\cos\chi \quad (3)$$

$$G = (f_0^2/kT)\mu_1\Delta\mu_{12}\cos\phi\cos\theta \quad (4)$$

$$H = f_0^2\Delta\mu_{12}^2 \quad (5)$$

$$I = f_0^2\Delta\mu_{12}^2\cos^2\theta \quad (6)$$

where μ_1 is the dipole moment of the electronic ground state, $\Delta\mu_{12}$ is the change of the dipole moment upon excitation to the Franck−Condon (FC) excited state, k is Boltzmann's constant, and T is the temperature. Because of the low symmetry of the compounds studied in this work, angles between the vectors of the ground-state dipole moment, μ_1, the dipole difference between ground and excited state, $\Delta\mu_{12}$, and the transition dipole moment, μ_{12}, have to be taken into account ($\phi = \angle(\mu_1, \mu_{12})$, $\chi = \angle(\mu_1, \Delta\mu_{12})$, $\theta = \angle(\mu_{12},\Delta\mu_{12})$). See the next section for a discussion of the local field correction, f_0. The EOAM spectra were evaluated by the usual regression analysis, and the EOAM coefficients are given in Table 3. These coefficients are not as meaningful for the dihydrazines because the first observed band corresponds to two overlapping transitions (see below), so these data appear in the Supporting Information.

Discussion

Calculations on Monohydrazine Optical Transitions. In an attempt to understand the observed quantities better, we have calculated the absorption bands of Hy[1]NA and Hy[2]NA and summarize the results of time-dependent density functional theory (TD-DFT)[12] calculations on the B3LYP/6-31+G* structures in Table 4. The bands are quite broad, and extend to about 24 000 cm^{-1} on the low energy side (see the ϵ versus $\tilde{\nu}$ plots in the Supporting Information). Because the calculation should be for the zero, zero vibrational transition, which is certainly significantly lower in energy than the band maximum, the TD-DFT predictions of $\tilde{\nu}$ for Hy[1]NA and Hy[2]NA look quite good. We also examined the estimates using Zerner's specially parametrized semiempirical method, ZINDO,[13] as implemented in Gaussian 98,[14] but it gives transition energies that are quite high (lowest energy transitions for B3LYP/6-31G+*-optimized Hy[1]NA and Hy[2]NA at 30 840 and 30 600 cm^{-1}, respectively, but these are for HOMO → LUMO + 1, and the HOMO → LUMO bands are calculated at an even less satisfactory 34 400 and 35 540 cm^{-1}).

The change in dipole moment vector is important for electron transfer considerations, but only the transition dipole moment tensor element, μ_{12}, is obtained in a single TD-DFT calculation. Cave and co-workers showed how to extract the $\Delta\mu_{12}$ vector from changes in the transition energy for calculations having a finite field applied (we followed Cave in using ±0.001 au in each principal direction).[15] The change in dipole moment vector, $\Delta\mu_{12}$, is calculated to be approximately parallel to the μ_1 vector (calculated angles $\chi = 31°$ for Hy[1]NA and 23° for Hy[2]NA). This is consistent with the transition corresponding a bridge reduction charge separation, that is, with the excited-state having more $^+$Hy−$^-$Ar character than the ground state. The transition dipole moment vector, μ_{12}, is calculated to be roughly parallel to the $\Delta\mu_{12}$ vector ($|\cos\theta|$ values corresponding to $\theta = 18°$ for Hy[1]NA, and 38° for Hy[2]NA), in reasonable agreement with experiment. The $\tilde{\nu}$ deviation amount, μ_{12}, is high, and the single available direction cosine for Hy[1]NA agrees better with experiment than those for Hy[2]NA. Cave pointed out to us that in his work charge-transfer bands with weaker overlap tended to get $\tilde{\nu}$ too small and, hence, $\Delta\mu_{12}$ too large.[15b]

As pointed out above, the α-naphthyl dihydrazines will be mixtures of syn and anti diastereomers, whereas their β-naphthyl isomers ought to also have contributions from diastereomers with the NN bonds syn to both the α and β' CH groups as well as unsymmetrical isomers. Semiempirical AM1 calculations are fast enough to allow comparing various diastereomers. They predict that despite the wide range of μ_1 values depending on relative orientation of one hydrazine unit with respect to the other the optical spectrum should be rather insensitive to the diastereomeric conformations present.[16] One diastereomer of each compound has been optimized using B3LYP/6-31G* (see the Supporting Information), but we have not done more sophisticated optical spectrum calculations because of the complexity of their excitations (see below).

Effects of Excited-State Intervalence on Absorption and Emission Spectra of bis-Hy-Substituted Naphthalenes. The bishydrazines appear at first glance to be very similar to the monohydrazines, but in fact the coupling between the two Hy to NA charge transfers introduces new features. In this section we discuss these features and the spectroscopic results briefly. We recently discussed such effects on the absorption spectrum of the dication oxidation state of an aryl-bridged bishydrazine[17] and of an *N*,*N*′-diphenylhydrazine radical cation.[18] Although they are very different structurally, each of these compounds has two chromophores attached to a bridge, so their transitions can involve either chromophore. This causes excited-state intervalence, as shown in cartoon form in Figure 3. The left side shows

TABLE 3: EOAM Regression Coefficients

compound	*E* (10^{-20} m^2 V^{-2})	*F* (10^{-40} C m^2 V^{-1})	*G* (10^{-40} C m^2 V^{-1})	*H* (10^{-60} C^2 m^2)	*I* (10^{-60} C^2 m^2)
Hy^{1}NA	423 ± 31	484 ± 30	505 ± 30	716 ± 130	523 ± 130
Hy^{2}NA	1277 ± 31	1173 ± 28	557 ± 28	2292 ± 105	1504 ± 105
Hy^{9}AN	747 ± 26	572 ± 19	565 ± 19	414 ± 87	394 ± 87

TABLE 4: Comparison of EOAM Results with Absorption Calculations

compound	Hy^{1}NA		Hy^{2}NA	
type of data	EOAM obsd	TD-DFT[a]	EOAM obsd	TD-DFT
$\tilde{\nu}$ (10^3 cm^{-1})	28.9	25.6[b]	28.3	27.4[c]
μ_1 (D)	2.6	1.76	2.1	2.22
μ_{12} (D)	2.19	2.07		1.49
$\Delta\mu_{12}$ (D)	5.3	9.3		9.4
$\lvert\cos\theta\rvert$ (μ_{12}, $\Delta\mu_{12}$)	0.86	0.95		0.81
$\lvert\cos\phi\rvert$ (μ_1, μ_{12})	0.69	0.90		
$\cos\chi$ (μ_1, $\Delta\mu_{12}$)	0.56	0.86		
c^2	0.12	0.21		0.02
$\Delta\tilde{\nu}$ (calcd (00)) −obsd (max)		−3.3		
μ_{12} (obsd/calcd)		1.1		
$\Delta\mu_{12}$ (obsd/calcd)		1.4		

[a] TD-DFT calculation on the B3LYP-6/31+G(d) optimized structure using Gaussian 98. [b] Calculated at 46% HOMO → LUMO, 1.1% (HOMO − 1) → LUMO. [c] Calculated at 45% HOMO → LUMO.

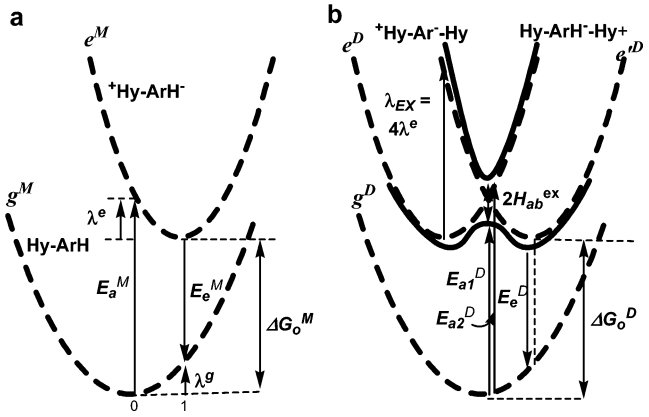

Figure 3. Classical two-state surfaces for charge separation in an aryl monohydrazine (a) and a dihydrazine (b). Note that electronic interaction in the excited state of the dihydrazine causes energy separation $2H_{ab}^{ex}$ at the ground-state geometry.

the monosubstituted hydrazine, for which the absorption transition energy (E_a^M) is determined by the energy difference between the relaxed ground state (a^M) and excited state (b^M), ΔG_o^M, plus the reorganization energy for the excited state (b), λ_b^M. The λ effective for emission is that of the ground state (a): $E_e^M = \Delta G_o^M - \lambda_a^M$. As indicated at the right side of Figure 3, there are two equal energy diabatic excited states for Hy_2Ar, $^+$Hy− $^-$Ar−Hy (e^D) and Hy-Ar$^-$−Hy$^+$ (e'^D), and there ought to be a significant electronic interaction between them that determines the barrier for hole transfer between the Hy units in the excited state, H_{ab}^{ex}, as indicated in the Marcus−Hush diagram. The absorption band for the dihydrazine ought to therefore consist of two overlapping bands having an energy separation of $2H_{ab}^{ex}$. Note that if H_{ab}^{ex} is significant then one expects both a splitting of the first absorption band and an emission band that is closer to the absorption band for the dihydrazine. We have also realized recently that the cartoon of Figure 3 is actually oversimplified and that four is the minimum number of states to consider for quantitative evaluation of

TABLE 5: Absorption and Emission Data (cm^{-1}) for Mono- and Dihydrazine Naphthalenes in Methylcyclohexane

compound	λ_{max} (nm)	E_a[a]	E_e	ΔE_{ae}	E_{ae}^{av}
Hy^{1}NA	344	29 100	19 500	9600	24 300
Hy_2^{14}NA	380	26 300	20 700	5600	23 500
Hy_2^{15}NA	360	27 800	17 900	9900	22 900
Hy^{2}NA	351	28 500	20 200	8300	24 350
Hy_2^{26}NA	372	26 900	22 000	4900	24 450
Hy_2^{27}NA	360	27 800	∼21 000	6800	24 400

[a] Caused by overlapping bands for the dihydrazines.

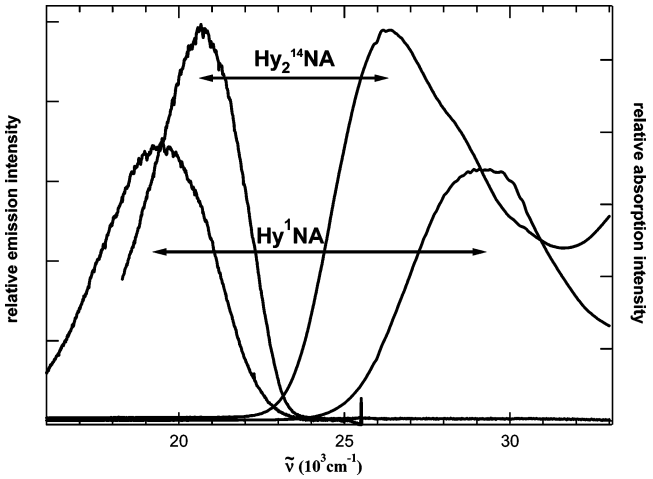

Figure 4. Comparison of absorption and emission spectra for Hy^{1}NA and Hy_2^{14}NA in methyl−cyclohexane.

electronic couplings in systems having two donating or releasing groups attached to a bridge, which we refer to as a neighboring orbital system.[19,20] Because we do not know a reasonable way to estimate the three transition energies necessary for these compounds, we will use only the "three-state" approach based on Figure 3 in this work.

The absorption and emission spectra for Hy^{1}NA and Hy_2^{14}NA are compared in Figure 4. As for the dihydrazine diradical dication hydrazine radical cation discussed previously,[17,18] there is a striking difference in the Stokes shift (ΔE_{ae}), the difference in absorption band maximum (E_a) and emission band maximum (E_e) for the monohydrazine (superscript M) and dihydrazine (superscript D), as predicted by the cartoon in Figure 3. Because the Hy unit releases electrons to the naphthalene ring, we would expect ΔG_o^D to be larger than ΔG_o^M. As indicated on the right of Figure 3, as the excited state $2H_{ab}^{ET}$ becomes significant, not only does E_{a1}^D decrease, as observed, but the minima on the double minimum excited-state surface pinch toward the middle of the diagram, which along with the increase in ΔG_o, will contribute to the observed increase in E_e^D.

Optical absorption and emission data for all of the Hy-substituted naphthalenes in methylcyclohexane are summarized in Table 5. The absorption maximum for Hy_2^{14}NA is 490 cm^{-1} higher in energy in methylcyclohexane, corresponding to a 6-nm red shift in the more polar dioxane than in the hydrocarbon solvent. As expected from the cartoon of Figure 3, ΔE_{ae} increases as the expected excited state, H_{ab}, decreases, leading to the ΔE_{ae} order Hy_2^{26}NA < Hy_2^{14}NA < Hy_2^{27}NA. Analysis

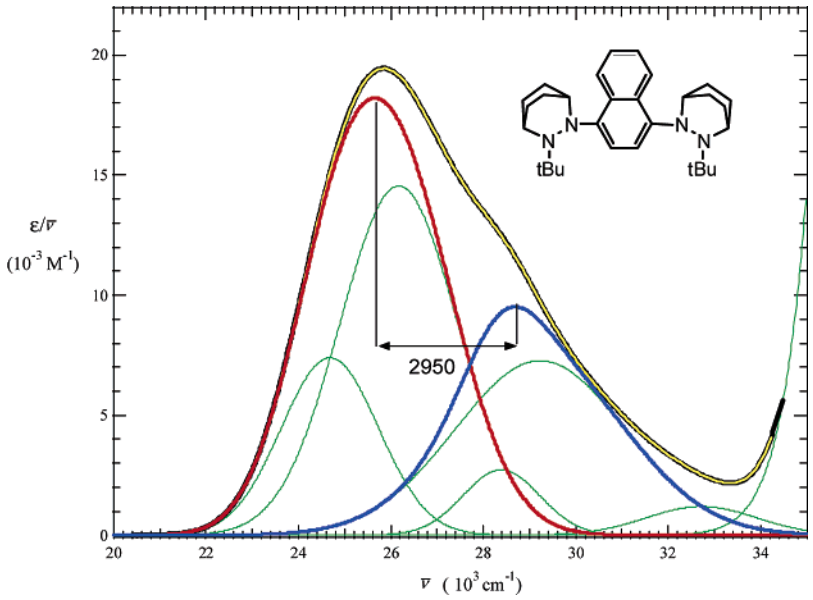

Figure 5. Six Gaussian fits (green curves) to the absorption spectrum of $Hy_2^{14}NA$ in dioxane to 34 500 cm^{-1} (black curve), sum of the green Gaussian fitting curves shown in yellow) using the sum of the lowest two Gaussians as the lower energy component (red curve), and the next two as the higher energy component (blue curve).

of the optical spectra of the ground-state radical cations, as will be discussed in detail elsewhere, gives the H_{ab} order $Hy_2^{26}NA^+ \approx Hy_2^{14}NA^+ > Hy_2^{15}NA^+ > Hy_2^{27}NA^+$.

In attempts to quantify the sub-band separation and intensity ratio, a multiple Gaussian fit to the absorption spectrum of $Hy_2^{14}NA$ (see Figure 5) gave bands having $\tilde{\nu}_l = 25\,640$ cm^{-1}, $\mu_{12}(l) = 0.78$ D, $\tilde{\nu}_h = 28\,590$ cm^{-1}, and $\mu_{12}(h) = 0.60$ D. This corresponds to an H_{ab}^{ex} value of 1470 cm^{-1}. However, bands this unresolved can be fit in several ways, depending upon the starting conditions. For example, when three or four Gaussians were used to simulate the low-energy absorption region of this $Hy_2^{14}NA$ spectrum in methylene chloride as two sub-bands in the same manner as the fit shown in Figure 5, we obtained five fits that had the μ_l/μ_u ratio averaging 1.38 (range −0.26 to +0.14) and ΔE averaging 3060 cm^{-1} (range −160 to +130); but by varying the starting conditions for the fits, a comparably good fit was obtained for three simulations that had the μ_l/μ_u ratio averaging 0.85 (range −0.07 to +0.08) and ΔE averaging 2800 cm^{-1} (range −94 to +25). We conclude that at least two sub-bands are present in this region, that the separation of upper and lower sub-bands is near 3000 cm^{-1}, and that their intensity ratio is not far from one. The methylene chloride spectral fits are thus entirely consistent with the dioxane spectrum in Figure 5 but demonstrate that we cannot be sure that the ratio of the sub-band intensities is greater than one. The dihydrazines with other substitution have even less distinct doubling of their first absorption band, and estimates of their splittings from multiple Gaussian fits are given in the Supporting Information (modeling not done as extensively in the other cases, and results for only $\mu_l/\mu_h < 1$ are included there).

The coupled states that produce the overlapping absorption bands are not amenable to simple interpretations of the electrooptical effects, and therefore we confine our analysis of the EOAM coefficients to the monosubstituted compounds in the next section.

Analysis of the EOAM Coefficients. Factor f_0 in eqs 2−6 represents the static local field correction that needs to be carried out using the above equations to account for the difference between the macroscopically applied field and the local field. f_0 might have been obtained using the Lorentz factor $(\epsilon_r + 2)/3$ with ϵ_r being the relative permittivity of the solvent, that is, a factor of 1.40 for dioxane ($\epsilon_r = 2.209$), the solvent used. However, solvatochromic measurements suggest that dioxane behaves more like a solvent with an ϵ_r value of 6. This effect can be taken into account applying the Onsager local field model where the local field factor is represented by a product of the cavity field factor, f^C, and the reaction field factor F^R.[21] For spherical cavities with radius a it is

$$f^C = 3\epsilon_r/(2\epsilon_r + 1) \tag{7}$$

$$F^R = 1/(1 - f^R\alpha) \tag{8}$$

$$f^R = 2(\epsilon_r - 1)/(4\pi\epsilon_0 a^3(2\epsilon_r + 1)) \tag{9}$$

Taking $\epsilon_r^m = 6$ for the microscopic permittivity in eq 9 and approximating the average solute polarizability, α, in eq 8 by the Clausius−Mosotti equation

$$\alpha = 4\pi\epsilon_0 a^3(\epsilon_r - 1)/(2\epsilon_r + 1) \tag{10}$$

yields the static local field correction

$$f_0 = f^C F^R = \epsilon_r(2\epsilon_r^m + 1)(n^2 + 2)/((2\epsilon_r + 1)(2\epsilon_r^m + n^2)) \tag{11a}$$

This equation simplifies to the Onsager expression

$$f_0 = f^C F^R = \epsilon_r(2\epsilon_r + 1)(n^2 + 2)/(2\epsilon_r + n^2) \tag{11b}$$

if $\epsilon_r = \epsilon_r^m$,as usual, and further to the Lorentz factor if additionally $\epsilon_r = n^2$ (apolar solvents). For dioxane ($n = 1.420$) eq 11b yields $f_0 = 1.52$, the value used in this work.

The EOAM coefficients may be interpreted as follows. E is a measure of the electrodichroism due to the alignment of the molecules in the externally applied electric field. This alignment is caused mainly by the interaction of the ground-state dipole moment, μ_1, with the applied field. Coefficients F and G describe the first-order Stark shift, and coefficients H and I describe the spectral broadening of the absorption band in the field. The shifts are proportional to the change of the dipole

TABLE 6: EOAM and Calculated Ground-State Dipole Moments

compound	$\lvert\cos\phi\rvert$ (μ_1, μ_{12})	$\cos\chi$ (μ_1, $\Delta\mu_{12}$)	$\lvert\cos\theta\rvert$ (μ_{12}, $\Delta\mu_{12}$)	μ_1(EOAM) D	μ_1(DFT) D	μ_1(AM1) D
Hy^1NA	0.69 ± 0.05	0.56 ± 0.15	0.86 ± 0.151	2.6 ± 0.6	1.76[a]	1.59
Hy^2NA			0.81 ± 0.04	2.1 ± 0.1[e]	2.22[a] (2.08[b,c])	1.59 (1.68[c])
Hy^9AN	0.69 ± 0.05	0.69 ± 0.16	0.98 ± 0.17	3.3 ± 0.6	2.03[a], 1.88[b]	1.58
				1.6 ± 0.1[d]		

[a] 6-31+G(d) basis set. [b] AM1 calculation. [c] Number in parentheses is for the less stable, NN bond syn to C_3 diastereomer, calculated to lie 0.52 kcal/mol higher in enthalpy by DFT (6-31G(d) basis set) and 0.27 higher by AM1. [d] Assuming $\cos\phi = 1$.

TABLE 7: Changes in Transition Dipole Moment upon Excitation Obtained from EOAM and the Electron Transfer Distances, c^2, and H_{ab}/λ Values Derived from Them and μ_{12}

compound	$\Delta\mu_{12}$, D	d_{12}, Å	d_{ab}, Å	c^2	H_{ab}/λ
Hy^1NA	5.3 ± 0.5	1.10 ± 0.10	1.43 ± 0.08	0.12 ± 0.02	0.16 ± 0.01
Hy^2NA	9.4 ± 0.2	1.97 ± 0.05	2.06 ± 0.04	0.023 ± 0.001	0.075 ± 0.002
Hy^9AN	4.0 ± 0.4	0.84 ± 0.09	1.27 ± 0.06	0.17 ± 0.02	0.19 ± 0.01

moment, $\Delta\mu_{12}$, upon excitation. The regression coefficients were analyzed as follows. A close equality of coefficients H and I and G and F indicates that the respective dipolar quantities in eqs 2−6 are nearly parallel. Table 4 includes these estimates of the cosines of the angles as well as an estimate of μ_1 (EOAM). It is found that the μ_{12} and $\Delta\mu_{12}$ vectors are nearly parallel for monohydrazines Hy^1NA and Hy^9AN. Nonzero angles appear to be present in Hy^2NA and in the dihydrazines, although there is substantial scatter in the estimates. The μ_1 (EOAM) value is also compared to the values calculated by time-dependent density functional theory (abbreviated TD-DFT) using B3LYP/6-31+G(d) for the monohydrazines and by AM1. The TD-DFT ground-state dipole moments, μ_1, are roughly aligned with the $N-C_{Ar}$ bonds (Hy^1NA: angle 26°, cos = 0.90; Hy^2NA: angle 23°, cos = 0.92, Hy^9AN: angle 22°, cos = 0.94). Thus, despite the substantial twist of the π system with respect to the lone pair of the nitrogen bonded to it, π-electron release to the naphthalene ring π system overcomes the σ-framework effect, which is in the opposite direction because N is more electronegative than C. The dihydrazine data are much less significant, both because the first absorption band contains two transitions and because of conformational mixtures (see the Supporting Information).

The $\Delta\mu_{12}$ values in Table 6 are obtained from eq 5 as $H^{1/2}/1.52$ (using the local field correction), and the values of electron separation distances on the adiabatic surfaces ($d_{12} = \Delta\mu_{12}/e$) and on the diabatic surface calculated using GMH theory[3] also appear. The $\Delta\mu_{12}$ and μ_{12} values are related to Mulliken's linear charge-transfer combination coefficient, c,[22] which is equal to the square root of the position of the minimum on the Marcus−Hush classical two-state model electron-transfer coordinate[2] (minima occur at c^2 and $1 - c^2$) by eqs 12−15,[23] where e is the electronic charge, which allows obtaining the ratio of

$$\mu_{12} = c(1 - c^2)^{1/2} e d_{ab} \tag{12}$$

$$\Delta\mu_{12} = (1-2c^2) e d_{ab} \tag{13}$$

$$c^2 = 1/2[1 - \Delta\mu_{12}(4\mu_{12}^2 + \Delta\mu_{12}^2)^{-1/2}] \tag{14}$$

$$H_{ab}/\lambda = [1 - (2c^{2-} 1)^2]^{1/2}/4 \tag{15}$$

H_{ab}, the electronic coupling between the Hy and Ar units, to the vertical reorganization energy (λ) using eq 15. The rather large c^2 and hence H_{ab} values make d_{ab} significantly larger than d_{12} and comparable to the 1.6 and 2.0 Å N_{Ar} to naphthalene ring central CC bond midpoint distances for Hy^1NA and Hy^2NA, respectively. Equations 12−15 use a simple two-state model that ignores direct overlap between the electron-transfer partners. There certainly is direct overlap, which may make this model inaccurate for estimating c^2 and H_{ab}.

Summary

Electrooptical absorption measurements establish that the lowest energy bands for Hy-substituted naphthalenes and anthracene correspond to electron transfer to an excited-state having a Hy^+NA^- charge distribution. The $\Delta\mu_{12}$ values provide estimates of the electron-transfer distances for charge separation on the diabatic surfaces using the two-state model of 1.4 Å for Hy^1NA and 2.1 Å for the less twisted Hy^2NA. These distances are comparable to the 1.6 and 2.0 Å distances between the nitrogen atom bonded to the aryl ring and the midpoint of the central naphthalene ring bond for Hy^1NA and Hy^2NA, respectively. The first absorption bands for the dihydrazines contain two transitions because of excited-state intervalence. The excited states may be described as resulting from electronic interaction between a $Hy^+-NA^--Hy^0$, $Hy^0-NA^--Hy^+$ pair. It is argued that excited-state electronic coupling is small enough in this case to produce a double minimum that qualitatively resembles that in the ground state of the disubstituted intervalence radical cations. The most noticeable consequence of the excited-state intervalence is a significantly smaller Stokes shift (difference between absorption and emission maximum) for the disubstituted compared to the monosubstituted compounds, under 60% as large for $Hy_2^{14}NA$ compared to Hy^1NA, and for $Hy_2^{26}NA$ compared to Hy^2NA. Multiple Gaussian fits to the absorption spectra produce estimates for the apparent excited-state electronic coupling of 1400 cm^{-1} for $Hy_2^{14}NA$, 1200 cm^{-1} for $Hy_2^{15}NA$, and significantly less, perhaps 850 cm^{-1} for $Hy_2^{26}NA$.

Experiments and Methods

Chemicals. For the electrooptical experiments, we dried the dioxane by distillation from an Na−K alloy under Argon prior to the preparation of solutions.

Optical and Electrooptical Absorption Measurements. The absorption spectra were recorded with a Perkin-Elmer 340 spectrophotometer. The electrooptical experiments were carried out as described in ref 23. For Gaussian calculations, we used Gaussian 98,[7] and for AM1 calculations we used VAMP.[8]

Hy^1NA, $Hy_2^{14}NA$, and Hy_2^9AN. We prepared Hy^1NA,[1b] $Hy_2^{14}NA$,[1b] and Hy_2^9AN [6] as described previously.

2-(2-*tert*-Butyl-2,3-diazabicyclo[2.2.2]oct-3-yl)-naphthalene (Hy^2NA). To an oven-dried 50-mL Schlenck flask under N_2, we added 2-bromo-naphthalene (0.103 g, 0.50 mmol). Et_2O (5 mL, freshly distilled from sodium benzophenone ketyl) was

added via syringe, at which point the solid dissolved. The flask was cooled to −78 °C and *t*-BuLi (1.7 M in pentane, 0.60 mL, 1.0 mmol) was added dropwise via syringe. The solution turned yellow and was allowed to stir for 2 h at −78 °C, after which 2-*tert*-butyl-2,3-diazabicyclo[2.2.2]oct-2-ene iodide (0.147 g, 0.50 mmol) was added. The solution was stirred for another 2 h at −78 °C, and then the cooling bath was lowered so the flask was no longer immersed in it, allowing a gradual warm-up. The solution was stirred for 2 more hours, after which the cooling bath was removed completely, and the solution was allowed to warm to room temperature while stirring overnight. The reaction was quenched with 25 mL of water and then extracted into 3 × 25 mL of toluene. The organic phases were combined, dried over $MgSO_4$, filtered, and the toluene evaporated, leaving 250 mg of brown oil. The oil was dissolved in 1 mL of acetone, placed in a test tube, AN was layered on top, and the test tube was placed in the freezer. Solid precipitated out overnight. It was filtered out and dried at 50 °C in a vacuum oven for 1 day, yielding an off white powder (80 mg, 32%). Further concentration of the mother liquor yielded an additional 39 mg (16%) of less pure material. Mp. 87−88 °C. MS: *m*/*e* 294.444539 (calcd for $C_{20}H_{26}N_2$, 294.4388). ^{1}H NMR (300 MHz, $CDCl_3$): δ 8.22−8.08 (m, 1H, Ar−H), 7.75−7.58 (m, 3H Ar−H), 7.41−7.16 (m, 3H, Ar−H), 3.87 (m, 1H NCH), 3.44 (m, 1H, NCH), 2.44−2.27 (m, 1H, CH_2), 2.05−1.87 (m, 2H, CH_2), 1.87−1.73 (m, 1H, CH_2), 1.70−1.52 (m, 4H, CH_2), 1.50−1.33 (m, 2H, CH_2), 1.31−1.18 (m, 2H, CH_2), 1.15 (s, 9H, $C(CH_3)_3$).

1,5-Diiodonaphthalene. 1,5-Diaminonaphthalene (1.067 g, 4,26 mmol) was suspended in 1.5 mL of concentrated H_2SO_4 and 25 mL of ice water. While stirring the suspension, $NaNO_2$ (1 g, 14.5 mmol) was added in 10 mL of H_2O and stirred for 30 min, during which time the solution turned from red (color of diaminonphthalene suspension) to brown/yellow to black. Urea (0.15 g, 0.25 mmol) was added to neutralize any remaining nitrous acid. The solution was filtered, and the resulting liquid was added slowly to a KI solution (5 g, 30.1 mmol in 50 mL of H_2O). This was stirred untill gas evolution was no longer evident. The solid was filtered off and recrystallized from acetone and water, following which it was dried in vacuum oven at 50 °C for 6 days to give 1,5-diiodonaphthalene as a tan solid (0.878 g, 34.2%). Mp. 145−146 °C (lit. 147 °C).[24]

1,5-Bis(2-*tert*-butyl-2,3diazabicyclo[2.2.2]oct-3-yl)naphthalene-1,5-diyl. ($Hy_2^{15}NA$). 1,5-Diiodonaphthalene was added to an oven-dried 50-mL Schlenck flask with a stirbar. Et_2O (5 mL, freshly distilled from sodium benzophenone ketyl) was added to that via syringe, and the resulting solution was cooled to −78 °C. The diiodide precipitated partially upon cooling. Cold *t*-BuLi (1.7 M in pentane, 1,2 mL, 2.04 mmol) was added dropwise via syringe and the solution turned orange/red and was allowed to stir for 1 h. 2-*t*-Bu-2,3-diazabicyclo[2.2.2]oct-2-ene iodide (0.297 g, 0.101 mmol) was added and the solution was stirred for 1 h at −78 °C before the cooling bath was lowered so that the flask was no longer immersed in it. The solution was allowed to stir for another hour, after which the cooling bath was removed completely, and the solution was allowed to warm to room temperature while stirring overnight. The reaction was quenched with 25 mL of water and extracted with 2 × 50 mL of toluene. The combined organic phases were dried over $MgSO_4$, filtered, and the toluene evaporated. Recrystallization from acetone and water afforded 36 mg and recrystallization of the crude left over, from toluene and AN, afforded another 68 mg. Total yield 104 mg (44.7%). Mp. decomposes at 287 °C. Ms: *m*/*e* 460.7136 (calcd for $C_{30}H_{44}N_4$, 460.7044), ^{1}H NMR (50 MHz, $CDCl_3$): δ 7.96−7.82 (m, 4H, Ar-**H**), 7.34−7.26 (m, 2H, Ar-**H**), 3.52 (br m, 2H, NC-**H**), 3.42 (m, 2H, NC-**H**), 2.45 (m, 2H, C-$\mathbf{H}_2$), 2.23 (m, 2H, C$\mathbf{H}_2$), 2.20 (m, 2H, C$\mathbf{H}_2$), 1.78 (m, 2H C$\mathbf{H}_2$), 1.68 (m, 2H, C$\mathbf{H}_2$), 1.60 (m, 2H, C$\mathbf{H}_2$), 1.46 (m, 2H, C$\mathbf{H}_2$), 1.16 (m, 2H C$\mathbf{H}_2$), 1.09 (s, 18 H, C(C$\mathbf{H}_3$)$_3$).^{13}C NMR {^{1}H} (125 MHz): δ 151.87 ($\mathbf{C}_{Ar}$), 151.82 ($\mathbf{C}_{Ar}$), 129.55 ($\mathbf{C}_{Ar}$), 129.26 ($\mathbf{C}_{Ar}$), 124.37 ($\mathbf{C}_{Ar}$-H), 124.20 ($\mathbf{C}_{Ar}$-H), 119.03 ($\mathbf{C}_{Ar}$-H), 118.34 ($\mathbf{C}_{Ar}$-H), 118.24 ($\mathbf{C}_{Ar}$-H), 118.10 ($\mathbf{C}_{Ar}$-H), 59.25 ($\mathbf{C}(CH_3)_3$), 53.22 (N**C**-H), 52.98 (N**C**-H), 46.59 (N**C**-H), 46.53 (N**C**-H), 29.44 ($\mathbf{C}H_2$), 29.24 ($\mathbf{C}H_2$), 29.06 (C($\mathbf{C}H_3$)), 26.93 ($\mathbf{C}H_2$), 23.34 ($\mathbf{C}H_2$), 23.14 ($\mathbf{C}H_2$), 21.10 ($\mathbf{C}H_2$), 20.79 ($\mathbf{C}H_2$).

2,6-Dibromonaphthalene. 2,6-Dibromonaphthalene was synthesized following the method of Shepherd.[25] A 250-mL three-neck round-bottom flask was fitted with a thermometer and a condenser (no cooling) with a vacuum adapter open to the atmosphere. Triphenylphospine (9.702 g, 36.99 mmol) in 30 mL of AN and Br_2 (1.95 mL, 37.85 mmol) were added to the flask. After stirring together, we added 2,6-dihydroxynaphthalene (2.942 g, 18.37 mmol) and the flask was subsequently immersed in a Woods metal bath. The solvent boiled off, and the resulting black solid melted and boiled gently. The internal temperature leveled off at 348 °C and was maintained for 6 min. The Woods metal bath was removed, and the contents of the round-bottom flask were suspended in refluxing EtOH. The EtOH was cooled and 6 N HCl was added to it to give a white precipitate. The precipitate was filtered out, recrystallized from EtOH, and dried in a vacuum oven for 2 days at 50 °C to give 2,6-dibromonaphthalene (0.926 g 17.6%). Mp. 158−159 °C (lit. 159−160 °C).[25] ^{1}H NMR (300 MHz, $CDCl_3$): δ 7.98 (d, J = 2.1 Hz, Ar−H), 7.64 (d, J = 8.7 Hz, Ar−H), 7.57 (d, J = 8.7 Hz, 2.1 Hz, Ar−H).

2,6-Bis(2-*tert*-butyl-2,3-diazabicyclo[2.2.2]oct-3-yl)naphthalene (Hy$_2^{26}$NA). 2,6-di-bromo-naphthalene (0.417 g, 0.518 mmol) was placed in an oven-dried 50-mL Schlenk flask under N_2. Et_2O (5 mL, freshly distilled from sodium benzophenone keytyl) was added and the solution was cooled to −78 °C. *t*-BuLi (1.7 M in pentane, 1.25 mL, 2.62 mmol) was added dropwise via syringe. No color change was observed. The solution was stirred for 2 h and then 2-tertbutyl-2,3-diazabicyclo-[2.2.2]oct-2-ene iodide (0.302 g, 1.03 mmol) was added. The solution was stirred for another 2 h, and the bath was lowered until the flask was not immersed, allowing the reaction to warm. After 2 more hours, the cooling bath was removed completely and the solution was allowed to warm to room temperature while stirring overnight. The reaction was quenched using 25 mL of H_2O and then extracted into 2 × 50 mL of toluene. The combined organic layers were dried over $MgSO_4$, filtered, and the solvent was removed with rotatory evaporation to yield a faint yellow powder. The solid was recrystallized from acetone and H_2O, resulting in a faint yellow powder (104 mg, 43.6%). MS: *m*/*e* 460.7136 (calcd, $C_{30}H_{44}N_4$ 460.7044). ^{1}H NMR (500 MHz, CDCl3): δ 8.11−7.95 (m, 1H, Ar-**H**), 7.58−7.39 (m, 2H, Ar-**H**), 7.24−7.03 (m, 2H, Ar-**H**), 3.78 (br s, 2H, NC-**H**), 3.41 (br s, 2H, NC-**H**), 2.33 (m, 2H, C$\mathbf{H}_2$), 1.95 (m, 4H, C$\mathbf{H}_2$), 1.78 (m, 2H, C$\mathbf{H}_2$), 1.59 (m, 4H, C$\mathbf{H}_2$), 1.40 (m, 2H, C$\mathbf{H}_2$), 1.22 (m, 2H, C$\mathbf{H}_2$), 1.14 (s, 18H, C(C$\mathbf{H}_3$)$_3$). Carbon peaks are broad and misshapen, implying a higher number of signals than actually listed because of a number of different diastereomers in solution. ^{13}C NMR{^{1}H} (125 MHz, C_6D_6): δ 152.42 ($\mathbf{C}_{Ar}$), 152.39 ($\mathbf{C}_{Ar}$), 130.94 ($\mathbf{C}_{Ar}$), 128.64 ($\mathbf{C}_{Ar}$-H), 127.73 ($\mathbf{C}_{Ar}$-H), 127.69 ($\mathbf{C}_{Ar}$-H), 127.43 ($\mathbf{C}_{Ar}$-H), 126.74 ($\mathbf{C}_{Ar}$-H), 122.17 ($\mathbf{C}_{Ar}$-H), 122.11 ($\mathbf{C}_{Ar}$-H), 122.06 ($\mathbf{C}_{Ar}$-H), 121.99 ($\mathbf{C}_{Ar}$-H), 116.71 ($\mathbf{C}_{Ar}$-H), 116.66 ($\mathbf{C}_{Ar}$-H), 58.90 ($\mathbf{C}(CH_3)_3$), 55.78 (N**C**-H), 55.74 (N**C**-H), 53.84 (N**C**-H), 53.79 (N**C**-H), 47.18 (N**C**-H), 46.76

(N**C**-H), 29.46 (C(**C**H$_3$)$_3$), 29.34 (C(**C**H$_3$)$_3$), 29.30 (**C**H$_2$), 27.11 (**C**H$_2$), 22.89 (**C**H$_2$), 22.78 (**C**H$_2$), 21.90 (**C**H$_2$), 21.56 (**C**H$_2$).

2,7-Bis(2-*tert*-butyl-2,3diazabicyclo[2.2.2]oct-3-yl)naphthalene-2,7-diyl (Hy$_2^{27}$NA). 2,7-diiodonaphthalene (0.190 g, 0.50 mmol) was added to an oven-dried Schlenk flask equipped with a stirbar. Et$_2$O (5 mL, freshly distilled from sodium benzophenone ketyl) was added via syringe and the resulting solution was cooled to −78°C. When cold, *t*-BuLi (1.7 M in pentane, 1.2 mL, 2.04 mmol) was added dropwise via syringe, upon which the solution turned orange. After stirring for 1 h, 2-tertbutyl-2,3-diazabicyclo[2.2.2]oct-2-ene iodide (0.296 g, 1.01 mmol) was added, and the solution was stirred for another hour. The cooling bath was then lowered so that the flask was no longer immersed, and the solution was allowed to stir for 1 h. The cooling bath was then removed, and the solution was allowed to warm to room temperature while stirring overnight. The reaction was quenched with 25 mL of H_2O, extracted into 2 × 50 mL of toluene, and the combined organic layers were then dried over $MgSO_4$. The drying agent was filtered out, and the solvent evaporated. The resulting solid was recrystallized from acetone and H_2O to give a white solid (102 mg, 44.3 %). MS: *m*/*e* 460.7136 (calcd, $C_{30}H_{44}N_4$ 460.7044). ^{1}H-NMR (500 MHz, $CDCl_3$): δ 7.93 (m, 2H, Ar-**H**), 7.49 (m, 2H, Ar-**H**), 7.22−6.93 (m, 2H, Ar-**H**), 3.84 (br s, 2H, NC-**H**), 3.42 (br s, 2H, NC-**H**), 2.43−2.32 (m, 2H, C**H**$_2$), 2.07−1.87 (m, 4H, C**H**$_2$), 1.86−1.72 (m, 2H, C**H**$_2$), 1.70−1.51 (m, 4H, C**H**$_2$), 1.50−1.32 (m, 2H, C**H**$_2$), 1.32−1.16 (m, 2H, C**H**$_2$), 1.15 (s, 18 H, C(C**H**$_3$)$_3$). Because of the high number of diasteromers in solution, the nuber of signals in the ^{13}C spectrum exceeds the number of carbons. ^{13}C-NMR, {^{1}H} (125 MHz, C_6D_6): δ 155.28 (**C**$_{Ar}$), 154.56 (**C**$_{Ar}$), 154.46 (**C**$_{Ar}$), 154.25 (**C**$_{Ar}$), 154.20 (**C**$_{Ar}$), 136.09 (**C**$_{Ar}$), 128.63 (**C**$_{Ar}$-H), 128.19 (**C**$_{Ar}$-H), 127.99 (**C**$_{Ar}$-H), 127.94 (**C**$_{Ar}$-H), 127.71 (**C**$_{Ar}$-H), 127.43 (**C**$_{Ar}$-H), 119.58 (**C**$_{Ar}$-H), 119.50 (**C**$_{Ar}$-H), 119.36 (**C**$_{Ar}$-H), 116.23 (**C**$_{Ar}$-H), 115.94 (**C**$_{Ar}$-H), 115.80 (**C**$_{Ar}$-H), 115.68 (**C**$_{Ar}$-H), 58.98 (**C**(CH$_3$)), 55.76 (N**C**-H), 55.45 (N**C**-H), 53.73 (N**C**-H), 53.68 (N**C**-H), 53.56 (N**C**-H), 47.23 (N**C**-H), 46.80 (N**C**-H), 29.46 (C(**C**H$_3$)), 29.36 (C(**C**H$_3$)), 29.26 (**C**H$_2$), 29.22 (**C**H$_2$), 27.10 (**C**H$_2$), 27.04 (**C**H$_2$), 22.86 (**C**H$_2$), 22.80 (**C**H$_2$), 22.71 (**C**H$_2$), 22.13 (**C**H$_2$), 22.05 (**C**H$_2$), 21.70 (**C**H$_2$), 21.65 (**C**H$_2$).

Acknowledgment. We thank the National Science Foundation for financial support of this work under grants CHE-9988727 and CHE-0240197. We thank Robert Cave (Harvey Mudd College) for patient instruction in how to extract $\Delta\mu_{12}$ from TD-DFT calculations.

Supporting Information Available: Crystal structural data for Hy^{1}NA and Hy^{2}NA, optical absorption spectra for the six Hy-substituted naphthalenes and emission spectra for the ones not shown in the text, and data from tables 3, 4, and 5 for the dihydrazines (analyzed as if they were a single absorption). This material is available free of charge via the Internet at http://pubs.acs.org.

References and Notes

(1) (a) Nelsen, S. F.; Ismagilov, R. F.; Powell, D. R. *J. Am. Chem. Soc.* **1997**, *119*, 10213−10222. (b) Nelsen, S. F.; Ismagilov, R. F.; Gentile, K. E.; Powell, D. R. *J. Am. Chem. Soc.* **1999**, *121*, 7108−7114.

(2) (a) Hush, N. S. *Prog. Inorg. Chem.* **1967**, *8*, 391−444. (b) Hush, N. S. *Coord. Chem. Rev.* **1985**, *64*, 135−157. (c) Marcus, R. A.; Sutin, N. *Biochim. Biophys. Acta* **1985**, *811*, 265−322. (d) Sutin, N. *Prog. Inorg. Chem.* **1983**, *30*, 441−499.

(3) (a) Cave, R. J.; Newton, M. D. *Chem. Phys. Lett.* **1996**, *249*, 15−19. (b) Cave, R. J.; Newton, M. D. *J. Chem. Phys.* **1997**, *106*, 9213−9226.

(4) Nelsen, S. F.; Ismagilov, R. F.; Trieber, D. A., II. *Science* **1997**, *278*, 846−849.

(5) Nelsen, S. F.; Newton, M. D. *J. Phys. Chem. A* **2000**, *104*, 10023−10031.

(6) Nelsen, S. F.; Ismagilov, R. F.; Powell, D. R. *J. Am. Chem. Soc.* **1998**, *120*, 1924−1925.

(7) Frisch, M. J.; Trucks, G. W.; Schlegel, H. B.; Scuseria, G. E.; Robb, M. A.; Cheeseman, J. R.; Zakrzewski, V. G.; Montgomery, J. A., Jr.; Stratmann, R. E.; Burant, J. C.; Dapprich, S.; Millam, J. M.; Daniels, A. D.; Kudin, K. N.; Strain, M. C.; Farkas, O.; Tomasi, J.; Barone, V.; Cossi, M.; Cammi, R.; Mennucci, B.; Pomelli, C.; Adamo, C.; Clifford, S.; Ochterski, J.; Petersson, G. A.; Ayala, P. Y.; Cui, Q.; Morokuma, K.; Malick, D. K.; Rabuck, A. D.; Raghavachari, K.; Foresman, J. B.; Cioslowski, J.; Ortiz, J. V.; Stefanov, B. B.; Liu, G.; Liashenko, A.; Piskorz, P.; Komaromi, I.; Gomperts, R.; Martin, R. L.; Fox, D. J.; Keith, T.; Al-Laham, M. A.; Peng, C. Y.; Nanayakkara, A.; Gonzalez, C.; Challacombe, M.; Gill, P. M. W.; Johnson, B. G.; Chen, W.; Wong, M. W.; Andres, J. L.; Head-Gordon, M.; Replogle, E. S.; Pople, J. A. *Gaussian 98*, revision A.9; Gaussian, Inc.: Pittsburgh, PA, 1998.

(8) (a) Dewar, M. J. S.; Zoebisch, E. G.; Healy, E. F.; Stewart, J. J. P. *J. Am. Chem. Soc.* **1985**, *107*, 3902−3909. (b) Our AM1 calculations were carried out using various versions of Clark's program VAMP: Rauhut, G.; Chandrasekhar, J.; Alex, A.; Steinke, T.; Clark, T. *VAMP 5.0*; Oxford Molecular, Oxford, U.K., 1994.

(9) Liptay, W. *Angew.* Chem., Int. Ed. Engl. **1969**, *8*, 177−188.

(10) (a) Gould, I. R.; Noukakis, D.; Gomez-Jahn, L.; Young, R. H.; Goodman, J. L.; Farid, S. *Chem. Phys.* **1993**, *176*, 439−456. (b) Gould, I. R.; Young, R. H.; Albrecht, A. C.; Mueller, J. L.; Farid, S. *J. Am. Chem. Soc.* **1994**, *116*, 8188−8199. (c) Although the Kodak group first used a larger factor,[3a] they very soon argued that the smaller factor, $3n^{1/2}/(n^2 + 2)$, is a better one to use[3b] but also cautioned that the true solvent effect is probably more complex.

(11) (a) Liptay, W. In *Excited States*; Lim, C., Ed.; Academic Press: New York, 1974; Vol. I, pp 129−229. (b) Wortmann, R.; Elich, K.; Lebus, S.; Liptay, W.; Borowicz, P.; Grabowska, A. *J. Phys. Chem.* **1992**, *96*, 9724−9730.

(12) (a) Burke, K.; Gross, E. K. U. In *Density Functionals*: Theory and Applications; Joubert, D., Ed.; Springer: Berlin, 1998, pp 116−146. (b) Stratmann, R. E.; Scuseria, G. E.; Frisch, M. J. *J. Chem. Phys. Chem.* **1998**, *109*, 8218−8224. (c) Takahasi, M.; Kira, M.; Sakamoto, K. Müller, T.; Apeloig, Y. *J. Comput. Chem.* **2001**, *22*, 1536−1541.

(13) (a) Zerner, M. C. In *Reviews of Computational Chemistry*; Lipkowitz, K. B., Boyd, D. B., Eds.; VCH: New York, 1991; Vol. 2, p 313. (b) Hanson, L. K.; Fajer, J.; Thompson, M. A. Zerner, M. C. *J. Am. Chem. Soc.* **1987**, *109*, 4728.

(14) (a) Zerner, M. C. In *Reviews of Computational Chemistry*; Lipkowitz, K. B., Boyd, D. B., Eds.; VCH: New York, 1991; Vol. 2, p 313. (b) Hanson, L. K.; Fajer, J.; Thompson, M. A. Zerner, M. C. *J. Am. Chem. Soc.* **1987**, *109*, 4728.

(15) (a) Cave, R. J.; Burke, K.; Castner, E. W., Jr. *J. Phys. Chem. A* **2002**, *106*, 9294−9305. (b) Private communication from R. J. Cave.

(16) (a) Blomgren, F.; Nelsen, S. F. *J. Org. Chem.* **2001**, *66*, 6551−6659. (b) For Hy$_2^{14}$NA$^+$, only a slightly larger N, Ar twist angle ϕ is estimated for the radical cation. For example, for the diasteromer with the *tert*-butyl groups syn and both NN bonds directed away from the center of the molecule the twist angles calculated by AM1 are $\phi^+ = 57.6°$, $\phi_0 = 52.8°$. These angles may be underestimated because the X-ray structure of Hy$_2^1$NA$^+$PF$_6^-$ gave $\phi^+ = 64.8°$.[19c] (c) Nelsen, S. F.; Konradsson, A. E.; Ismagilov, R. F.; Guzei, I. A. *Cryst. Growth Des.*, in press; cg050154w.

(17) Lockard, J. V.; Zink, J. I.; Konradsson, A.; Weaver, M. N.; Nelsen, S. F. *J. Am. Chem. Soc.* **2003**, *125*, 13471−13480.

(18) Lockard, J. V.; Zink, J. I.; Trieber, D. A., II.; Konradsson, A. E.; Weaver, M. N.; Nelsen, S. F. *J. Phys. Chem.* **2005**, *109*, 1205−1215.

(19) For the neighboring orbital model applied to dinitroaromatic radical anions, see Nelsen, S. F.; Weaver, M. N.; Zink, J. I.; Telo, J. P. *J. Am. Chem. Soc.* **2005**, *127*, 10611−10622.

(20) For the neighboring orbital model applied to diaminoaromatic radical cations, see Nelsen, S. F.; Luo, Y.; Weaver, M. N.; Lockard, J. V.; Zink, J. I. *Beyond the Two-State Model: Optical Spectra of Protected Diamine Intervalence Radical Cations Related to N,N,N′,N′-Tetralkylbenzidine*; to be published.

(21) Wortmann, R.; Bishop, D. M. *J. Chem. Phys.* **1998**, *108*, 1001−1007.

(22) Mulliken, R. S. *J. Am. Chem. Soc.* **1952**, *74*, 811−824.

(23) (a) Maslak, P.; Chopra, A.; Moylan, C. R.; Wortmann, R.; Lebus, S.; Rheingold, A. L.; Yap, G. P. A. *J. Am. Chem. Soc.* **1996**, *118*, 1471−1481. (b) Wortmann, R.; Wurthner, F.; Sautter, A.; Lukaszuk, K.; Matshciner, R.; Meerholz, K. *Proc. SPIE-Int. Soc. Opt. Eng.* **1998**, *3471*, 41−49. (c) Wortmann, R.; Poga, C.; Twieg, R. J.; Geletneky, C.; Moyan, C. R.; Lundquist, P. M.; DeVole, R. G.; Cotts, P. M.; Horn, H.; Ricke, J. E.; Burland, D. M. *J. Chem. Phys.* **1996**, *105*, 10637−10647.

(24) Kawasaki, M.; Lee, S. J.; Bersohn, R. *J. Chem. Phys.* **1977**, *66*, 2647−2655.

(25) Shepherd, M. K. *J. Chem. Soc.*, Perkin Trans. 1 **1994**, 1055.